ELSEVIER

Journal of Nuclear Materials 295 (2001) 167–178

journal of nuclear materials

www.elsevier.nl/locate/jnucmat

Molecular dynamics modeling of irradiation damage in pure and uranium-doped zircon

Jean-Paul Crocombette [a,*], Dominique Ghaleb [b]

[a] CEA, CEREM-SRMP, CE Saclay, 91191 Gif sur Yvette cedex, France
[b] CEA, DCC/DRRV/SCD, CE Valrho BP171, 30207 Bagnols-sur-Cèze cedex, France

Received 13 September 2000; accepted 19 March 2001

Abstract

Molecular dynamics (MD) with empirical potentials of the Born–Mayer–Huggings (BMH) type has been used to study irradiation damage in pure and uranium-doped zircon ($ZrSiO_4$). Displacement threshold energies (DTE) have been calculated and displacement cascades (DC) initiated by α-decay recoil nuclei have been modeled. A DC directly produces an amorphous core inside the cascade track, with a structure identical to the one of fully amorphous material. The analysis of the disorder of cations first neighbors shell shows that the cascade track has a concentrical shape with decreasing disorder from the core to the outer shell of the track. In the amorphous zone, some silicon atoms are connected to each other, indicating the appearance of SiO_2-rich and ZrO_2-rich nanophases. © 2001 Elsevier Science B.V. All rights reserved.

PACS: 02.70.Ns; 61.80.Jh; 61.82.Ms

1. Introduction

Zircon ($ZrSiO_4$) is a mineral of high interest for nuclear industry. Indeed it is considered as an actinide bearing phase for nuclear waste management, especially for weapons-grade plutonium or UO_2 spent fuel in the United States [1]. In France, due to its simple structure and chemical composition, it is regarded as a model material for possible new actinides confinement matrices. Actinides confining material will be subject to α-decay damage. α disintegrations are characterized by the emission of an α particle and a recoil nucleus. The α particle initially has an energy of 4–6 MeV. It dissipates most of its energy by ionization processes and only produces a few hundred of isolated atomic displacements along its path. On the opposite, nearly the whole all energy of the recoil nucleus is lost through elastic collisions with atoms in the structure, producing displacement cascades (DC) of a few thousand atoms resulting in highly localized damage [2]. These DC are the subject of the present study. With accumulating α-decay damage, zircon undergoes a radiation induced transition to an amorphous (or metamict) state. Such metamictization appears in many minerals considered for actinides storage [3]. In this context, the amorphization of zircon has important drawbacks: it causes an important swelling of the material [4] along with a decrease in hardness (40%) and bulk modulus (60%) [5]. Both swelling and hardness decrease strongly modify the mechanical behavior of zircon matrices. Moreover, the leaching rate of zircon rises dramatically with increasing metamictization. Fully amorphous zircon has a leaching rate (1.8×10^{-6} g cm^{-2} day^{-1}) sixty times larger than crystalline material (2.9×10^{-8} g cm^{-2} day^{-1}) which leads to an important increase in actinides loss rates [6]. Experimentally it is known that above 1960 K zircon totally decomposes into ZrO_2- and SiO_2-rich phases [7]. In natural metamict zircons no decomposition can be seen, but metamict zircons commonly experience a partial or complete decomposition upon annealing prior to recrystallization (see [8] and references therein). Direct decomposition under irradiation at high temperature

* Corresponding author.
E-mail addresses: jpcrocombette@cea.fr (J.-P. Crocombette), dghaleb@cea.fr (D. Ghaleb).

PII: S0022-3115(01)00557-8

has also been observed in an ion bombardment experiment [9]. Such decomposition, if it happened in an actinide disposal context, would greatly affect the retention properties of the material. Actinides being poorly accommodated in quartz or zirconia, an accumulation of radioactive material would occur along the grain boundaries or at the frontier between the different phases. Such an accumulation would enhance diffusion as it would proceed through shortcuts in grain boundaries and thus lead to actinide release.

In spite of many experimental studies on radiation effects in zircon [10], little is known about the elementary processes of radiation damage and induced amorphization or decomposition. We aim in this study to obtain, by molecular dynamics (MD) simulation, some information, at atomic level, about the DC created along the recoil nucleus trajectory by atomic collisions and about the structural modifications due to these cascades in pure and uranium-doped zircons. MD simulation has the great advantage that it permits the realistic treatment of the atomic motions and naturally include the crystal structure effects. With this method, it is therefore possible to calculate the displacement threshold energies (DTE) needed as an input for more macroscopic models e.g. as binary collisions models such as TRIM [11]. One can also reproduce all the atomic movements that take place during the DC. The main disadvantage is that such simulations are computationally very demanding. As a consequence only quite small impulsions for the primary knocked on atom (PKA) can be considered. Moreover, the simulated time is limited to a few tens of picoseconds. It is not possible within MD simulation to predict the long term response, dominated by diffusion events, of the material. However, a good description of the elementary processes during the DC and in the next picoseconds proves necessary to understand the irradiation damages on the whole.

The paper is organized as follow: first the empirical potentials we used are described and their validity is assessed. In the next part DTE in zircon are calculated and analyzed. The following part deals with DC modeling. Some specific details of methodology of DC modeling are given, then results concerning DC unfolding and the structure of the cascade tracks are presented. In the discussion part, some information relevant to amorphization and decomposition are drawn from our results.

2. Empirical potentials

2.1. Parameters

We use empirical potentials to mimic the interaction between ions in zircon. A very accurate description of mineral structures can be obtained using empirical potentials. The best empirical potentials include the ion polarization effects, for instance by using a shell model [12] in which the electronic cloud is linked to the core ion by a spring of constant stiffness. But DC cannot be modeled with such a kind of potentials. Indeed, under ballistic collisions, some ion cores experience a very fast increase of their kinetic energies. As electrons shells do not experience such collisions, an artificial and unrealistic separation appears between the ion cores and their electron shell. Therefore it is not possible for DC modeling to separate the position of the electrons shells and of their ion cores. Hence, only empirical potentials of the rigid ion model type can be used. We chose two-bodies empirical potentials of the Born–Mayer–Huggins (BMH) type for our simulations. For each pair of atom types i–j the interaction potential:

$$\phi_{ij} = b\left(1 + \frac{q_i}{n_i} + \frac{q_j}{n_j}\right)\exp\left(\frac{\sigma_i + \sigma_j + -r_{ij}}{\rho_{ij}}\right) + \frac{1}{4\pi\varepsilon_0}\frac{q_i q_j}{r_{ij}},$$

where q_i and q_j are the formal charges of ions i and j (i.e., $+4$ for cations and -2 for oxygen); n_i and n_j are the numbers of valence shell electrons ($n_i = 8$ for all ions in our case). b, ρ_{ij} and σ_i are adjustable parameters (see Table 1). The first part of the potential is a short range repulsion, the second part is the long range Coulomb interaction. The cut-off radius of the exponential term is 6.7 Å. The Coulomb term has been calculated thanks to an Ewald summation technique [13] with an interaction range (Ewald parameter) η of 4.36 Å. The cut-off radius in real space for this term is 11.2 Å. In reciprocal space the summation on $\vec{K}$ vectors has been made on all vectors with components K_u smaller than $5 \times \pi/L_u$, where L_u is the dimension of the box along the u dimension ($u = x$, $y$or z). MD, using the standard Verlet algorithm [14], and conjugate gradient energy minimizations were performed with a code used for simulating DC in metals and nuclear glasses developed by Doan [15] and Delaye [16–18]. The parameters of the potentials were taken equal to those used by Delaye [16] except for σ_{Zr} which was reduced by 10% to ensure a better

Table 1
Parameters used for pair potentials

$b = 0.221$ eV; $\rho_{ij} = 0.29$ Å except $\rho_{O\text{-}O} = 0.35$ Å and $\rho_{U\text{-}O} = 0.40$ Å; $C_{U\text{-}O} = 65.4$ eV Å^6				
	Si	O	Zr	U
σ (Å)	1.11	1.42	1.31	2.019

agreement with experimental data. The uranium ions (U^{4+}) interact with surrounding ions with the same potentials than the other ions, except that a supplementary term ($-C/r^6$), which represents the dipolar interactions between the atoms, has been introduced for uranium–oxygen interactions [18]. During the DC, atoms can get very close to each other. In this case their interaction, for interatomic distances smaller than 1 Å, is represented by a Ziegler potential [11]. The two kinds of potentials are connected (between 0.9 and 1.0 Å) with a fifth order polynomial to ensure continuity of the potential and of its two first derivatives.

2.2. Validation of the potentials

The validity of the potentials has been checked on the structure of zircon [19] and the formation energies of point defects [20]. The zircon tetragonal structure, space group $I_{4_1/amd}(D_{4h}^{19})$, consists of dodecahedral ZrO_8 groups forming edge-sharing chains parallel to the *a* axis and distorted SiO_4 tetrahedral monomers forming edge-sharing chains with alternating ZrO_8 groups parallel to the *c* axis [21]. In a perfect box without surface nor defect, zircon remains crystalline in our calculations up to 2500 K. Moreover, calculated characteristics of numerically quenched zircons exhibit good agreement with experimental values from both microscopic and macroscopic points of view (see Table 2). The *c*/*a* ratio is poorly reproduced. An accurate description of the electronic structure of the compound (including an extended k point sampling of the Brillouin zone) proves necessary to get a correct value of the *c*/*a* parameter [19]. The quite high SiO_4 tetrahedra distortion is only partially reproduced by our pair potentials. In common silica structures, the tetrahedra are much less distorted and it is of common practice to introduce three-body terms to favor *perfect* O–Si–O angles. In the case of zircon the introduction of these terms would only worsen the results as the distortion are underestimated by our pair potentials.

Intrinsic point defects (Frenkel pairs, Schottky and anti-Schottky defects) formation energies have been calculated and compared with ab initio electronic structure calculations [20]. This proves a good way to further assess the validity of our empirical potentials. The formation energies estimated with empirical potentials are of the correct order of magnitude but are larger than energies calculated from first-principles by a factor ranging from 1.5 to 1.9 (see Table 3). Simulated zircon therefore proves stable as regards the introduction of point defects, which is quite satisfactory. The overestimation of the formation energies should mainly be due to the fact that the empirical potentials deal with formal charges and thus neglect the departure from the ionic configurations due to the partial covalency of the bonding.

3. Displacement threshold energies

DTE are important parameters that control the amount of radiation damage in a material [22]. They are defined, for each ion type, as the minimum amount of kinetic energy that should be transferred to an ion to permanently displace it from its original site. These quantities can be measured experimentally by various techniques such as optical and thermally stimulated spectroscopies, electron paramagnetic resonance, positron annihilation and electron microscopy. They are also important parameters for the modeling of irradiation damage accumulation by binary collision models such as TRIM [11].

Table 2
Comparison between calculated and experimental (in parenthesis) structural characteristics of zircon (from [19])

Si–O distance (Å)	Zr–O distance (Å)	O–Si–O angle	Equilibrium volume (Å^3)	c/a ratio	Bulk modulus (Gpa)
1.59 (1.62)	2.16 (2.13) 2.36 (2.27)	101° (97) 113° (116)	115 (116)	0.99 (0.91)	167 (225)

Table 3
Point defect formation energies (E_f) in zircon (in eV)[a]

E_f	O_{FP}	Si_{FP}	Zr_{FP}	Schottky	AS
Empirical potentials	14.1	33.3	36.3	61.7	64.6
DFT-LDA	7.3	22.9	24.0	34.1	41.8
Ratio	1.93	1.45	1.51	1.79	1.53

[a] Comparison between BMH empirical potentials and ab initio electronic structure results (from [20]). O_{FP}, Si_{FP} and Zr_{FP} denote the oxygen, silicon and zirconium Frenkel pairs, respectively. Schottky stands for the Schottky defect (6 vacancies) and AS denote the 'anti-Schottky defect' (6 interstitials). The last line indicates the ratio between values calculated by empirical potentials and by ab initio calculations.

In MD simulation DTE can be easily calculated, for each ion type, by giving, in various directions, a series of impulsions of increasing kinetic energy to an atom of the chosen type and following the subsequent atomic motions. In each direction, for low energies, after some atomic displacements, the knocked-on atom and all the other displaced atoms readily return to their original positions, leaving the crystal unperturbed. Beyond a certain energy the knocked-on atom does not return to its original site. In this case, at least one (sometimes more) Frenkel pair remains at the end of the simulation. The DTE of the given ion type is then the minimum among the various directions of these threshold energies. Another, conceptually less direct but computationally less demanding, method exists to calculate the DTE with empirical potentials. One determines, through a series of static calculations, the saddle point for the displacement of an atom from its original site to an interstitial position. The energy increase at the saddle point gives an estimation of the DTE. However using static calculation may lead to inaccurate description of the pair creation process. For instance, in some cases, the vacancy–interstitial pair is dynamically *unstable*. Dynamical calculations in these cases directly lead to their recombination. Static calculations do not allow such recombinations and therefore underestimate the DTE. Thus we think that dynamic calculations, even if they are heavier than static ones, lead to more reliable values for the DTE as they directly reproduce the physical process of Frenkel pair formation. For this reason, we chose to estimate the DTE in zircon using the dynamical procedure.

The calculation has been carried out in the NVE ensemble using a box containing 5184 atoms initially in a crystalline arrangement. It was ended after a simulated time of 0.3 ps. Longer simulations performed for some test cases showed that such a short simulated time was indeed sufficient, no subsequent evolution being noticeable. The Frenkel defect has then reached an energetically *metastable* configuration (i.e., subsequent recombinations of the vacancy–interstitial pair remains possible by a thermally activated diffusion process). The obtained values for DTE in pure zircon are indicated in Table 4. Few experimental figures are at our disposal to compare with our calculated values. On zircon itself only the DTE of zirconium has been estimated. It should lie between 41 and 97 eV [23]. For silicon in SiC the DTE is between 18 and 53 eV [22], and for oxygen in different ceramics it ranges between 20 and 70 eV [22]. Our calculated values are compatible with these experimental estimations. They are compared in Table 4 with the results of static calculations [24,25] which are in general agreement with our figures except for the silicon DTE. Beyond the differences in potentials, the main source of divergence lies in the method used to calculated the DTE. As expected, static calculations lead to smaller values. Nevertheless, the imprecision due to the empirical potentials should be kept in mind. With the empirical potentials used in the present study, Frenkel pair formation energies are overestimated by a factor 2 for oxygen and 1.5 for cations (Table 3). So our calculated values may be overestimated by a comparable amount. They should in any case be regarded as an upper limit for real DTE. One can see that the cation DTE are much larger than the oxygen one. The assumption that is sometimes done in binary collision model that all DTE are equal in a given compound is therefore wrong in the present case. This difference may come from the fact that the cations are encapsulated in the shell of oxygen first neighbors. The destruction of this shell (needed for creating a cation Frenkel pair) costs quite a lot of energy.

Table 4
Calculated DTE in zircon (in eV)

	Zr	Si	O
Present calculation	90	98	32
Williford et al. [24]	90	20	53
Meis [25]	76	85	38

4. Displacements cascades

4.1. Uranium doping

DC were modeled in pure and uranium-doped zircons. Uranium atoms have been placed in substitution for zirconium atoms. The simulation box used in DC modeling contains 139968 atoms built from the repetition, 18 times in each direction, of the 24 atom conventional unit cell of zircon. In this box three different amounts of uranium doping have been considered which correspond to three slightly different materials. In the first kind of box only one zirconium atom (on a total of 23328 zirconium atoms) is substituted by an uranium atom. This corresponds to what may happen in a natural mineral of small uranium content. In the second (resp. third) boxes 1000 (resp. 3000) uranium atoms have been randomly introduced so that 4% (resp. 12%) of the zirconium atoms have been substituted, which corresponds to a weight ratio of uranium dioxide of 6.1% (resp. 18.3%). These are closer to the possible situation of high level wastes where the actinide percentages, at present not well defined, should be quite large. Once numerically relaxed at constant ambient pressure the three boxes differ in sizes (see Table 5). The introduction of large uranium ions increases the volume of the box by a factor of 1.9% (resp. 5.6%) for 4% (resp. 12%) atomic doping. One can see that the volume increase varies linearly with doping (Vegard's law).

Table 5
Characteristics of the calculated DC

DC number	1	2	3	4	5
U doping	Pure zircon		4%U		12%U
Size of the box (nm)	$11.43 \times 11.43 \times 11.32$		$11.52 \times 11.52 \times 11.37$		$11.67 \times 11.67 \times 11.47$
PKA energy (keV)	4.0	5.0	4.0	5.0	5.0
Cooling time (ps)	5	6	6	8	9
PKA trajectory length (nm)	4.8	3.7	4.1	3.2	5.2
Number of displaced atoms	Si:24	Si:72	Si:22	Si:38	Si:63
	O:214	O:413	O:219	O:322	O:389
	Zr:14	Zr:54	Zr:14	Zr:32	Zr:49
			U:1	U:2	U:6
Number of disordered atoms	Si:26	Si:59	Si:41	Si:53	Si:69
	Zr:84	Zr:176	Zr:101	Zr:174	Zr:174
			U:6	U:7	U:8
Number of distorted atoms	Si:71	Si:121	Si:55	Si:121	Si:108
	Zr:59	Zr:85	Zr:58	Zr:67	Zr:8
			U:1	U:3	U:5
Swelling	+0.13%	+0.16%	+0.02%	+0.05%	+0.06%
Stored energy (eV)	302	479	200	314	251
Stored energy per atom (eV/at)	0.60	0.45	0.31	0.29	0.23

4.2. DC modeling methodology

To initiate the DC, an impulsion is given to an uranium atom. Introducing this perturbation leads to a series of atomic collisions. We follow the movements of the atoms inside the simulation box until a metastable state is reached (for the time scales of our simulations i.e., picoseconds). Primary impulsions corresponding to kinetic energies of 4 and 5 keV have been considered. These energies are smaller than expected in real materials (around 70 keV) but they correspond to the maximum that we can tackle with our computer resources. The cascades have been calculated at constant volume. The average of the kinetic energies has been regularly calculated. It can be related to the temperature. In principle, this relation holds only for thermodynamical equilibrium but for convenience we shall still speak in terms of temperature. At the beginning of the simulation the crystal is in thermal equilibrium at 300 K. Afterwards the temperature of a 0.3 nm wide external layer is kept constant at 300 K to model the thermal bath constituted in reality by the outer part of the crystal. For this purpose, the velocities of the atoms in the outer layer are regularly rescaled to maintain the kinetic energy calculated as an average on all atoms in the layer at a constant value of 300 K. After the DC, in order to analyze the shape of the DC track, the box has been quenched, using a conjugate gradient algorithm, at constant pressure. We used a Parinello–Rahman-like algorithm [26], keeping the tetragonal shape of the box (i.e., maintaining constant angles), and adding a dissipation term on its movements. The mass of the box has been fixed to half the sum of the masses of the atoms contained in it. At the beginning of the cascade, the velocities of the ions can reach quite high values. It is therefore necessary to use a time step as short as 10^{-5} ps to discretize the trajectories of the ions. After some 10^{-3} ps, the maximum atomic velocity decreases and the time step of the simulation can be increased. This was accomplished routinely by adjusting the time step so that the maximum atomic displacement between two consecutive time steps is smaller than 0.05 Å. Starting from 1×10^{-5} ps it rises to 2×10^{-3} ps. The total simulation time for the DC is 10 ps.

4.3. DC unfolding

In the primary stage of the DC the crystal is violently disturbed. Many atoms are displaced from their original position. Nevertheless a very quick recovery process takes place and half the atoms displaced by more than 1 Å eventually recover their original positions in less than 1 ps. We monitored the possible occurrence of collective movements of the silicon tetrahedra as such movements are known to occur in glasses [17]. We found out that this kind of movements never occurred in our simula-

tions: no displaced silicon atoms has the same four oxygen neighbors before and after the cascade.

Thanks to the large size of the simulation box, the global temperature rises only up to 600 K during the unfolding of the DC. This maximum temperature is reached in less than one tenth of a picosecond. Then temperature gently decreases during the rest of the simulation to reach values close to the fixed external layer value. To illustrate this point, the time at which temperature decreases to 350 K is given in Table 5. In the vicinity of the DC the temperature is much higher. The simulation box has been divided in one thousand small cells. The local temperature has been estimated in each cell. After 0.1 ps the temperature, in the cell in which the projectile is located, is about 25 000 K. In the cells directly close to it, it ranges from 3000 to 10 000 K. The temperature in this zone remains higher than 3000 K up to nearly 1 ps. It then decreases to 2000 K at 1.5 ps and 1000 K at 2.5 ps. The rate of this decrease depends on the size of the simulation box and on the width of the controlled temperature peripheral area. In reality, the local temperature probably decreases more slowly.

4.4. Structure of the cascade tracks

A cascade results in the creation of an amorphous track (see Fig. 1). This behavior is very different from what is observed in metals where DC tracks can be analyzed in terms of assemblies of point defects. In the case of zircon the center of the cascade track is obviously no longer crystalline. No isolated point defect appears. The shape of this track is roughly cylindrical along the path

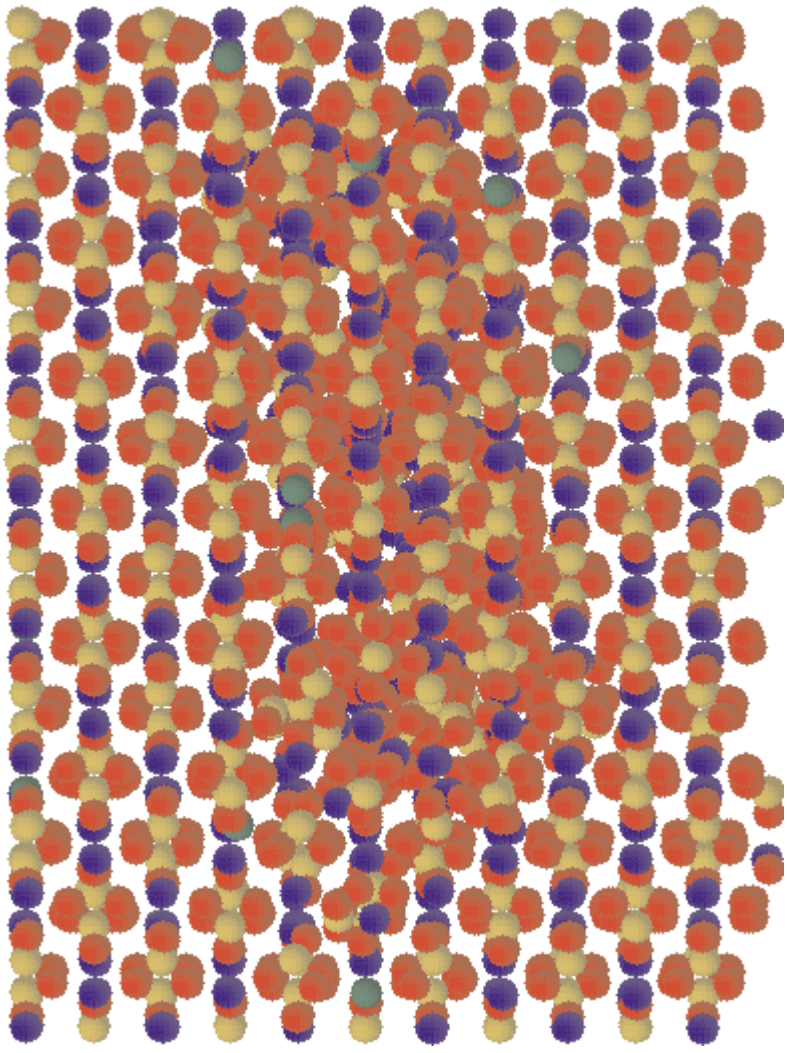

Fig. 1. Morphology of a 4% U-doped zircon crystal after a 5 keV DC; Si (yellow), O (red), Zr (blue), U (green).

of the primary atom. Nevertheless, the disorder is larger near the end of the projectile trajectory. Usual tools for DC tracks analysis in metals make a distinction between replacement (in which an atom takes the place of an equivalent atom in the crystalline structure) and displacement (an atom occupies an interstitial position at the end of the cascade). The tracks calculated in zircon cannot be analyzed in these terms as they are completely amorphous and it is not possible to define the occupancy of the crystal sites in the track after the cascade. Therefore it is not possible to define replacements events. In order to measure the number of atoms that experience a displacement during the cascade we simply define as displaced the atoms that have traveled more than 2 Å from their original site to their final position at the end of the simulation. This distance was chosen because it is the average of first neighbors interatomic distances (cf. Table 1). Applied in a case where crystal structure is preserved, this definition would include both displaced and replaced atoms. The obtained figures are indicated in Table 5. They exhibit a decrease as a function of the atomic mass and an increase as a function of the projectile primary energy. The distance covered by the projectile is of the order of 4 nm (see Table 5). The fact that the 4 keV cascades result in longer trajectories is due to the difference in projectile initial direction. For the 5 keV cascade the impulsion was given in the $[1,1,1]$ direction so that the projectile had to cross the dense planes of the zircon structure directed in the $[1,0,0]$ and $[0,1,0]$ directions. The 4 keV impulsion was directed along the $[1,1,10]$ direction, i.e., nearly in the direction of the empty cylinders that exist in the structure in the $[0,0,1]$ direction. The larger trajectory length in these cases is the evidence for canalization of the projectile in the $[0,0,1]$ direction.

The structure of quenched DC tracks have been analyzed. Two tests, based on the consideration of the first neighboring shell of the atoms, were used to quantify the local disorder around the cations. For each cation, we

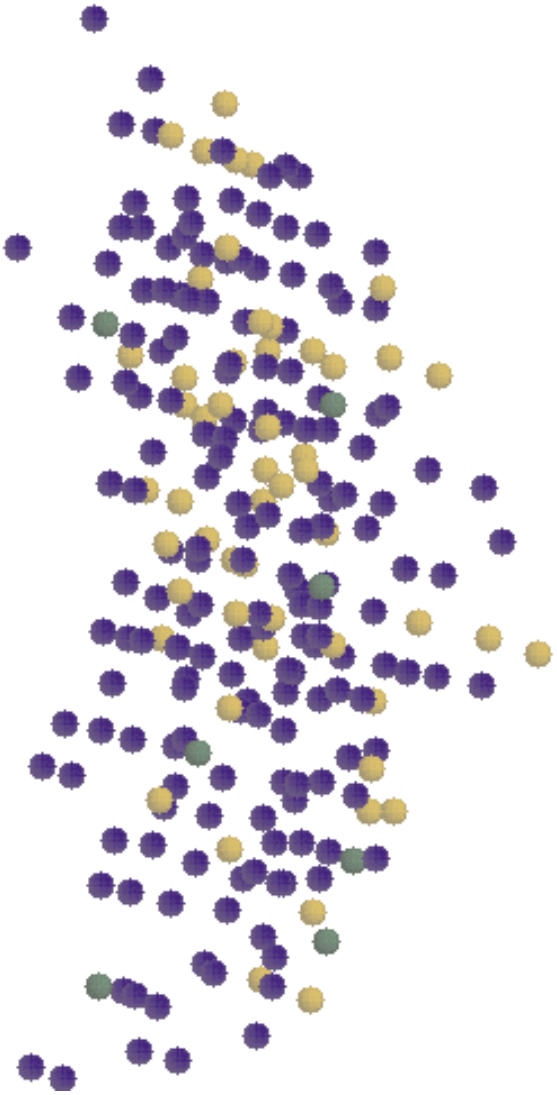

Fig. 2. Disordered cations after the DC (cations with a different number of neighbors than in the perfect crystal); Si (yellow), Zr (blue), U (green).

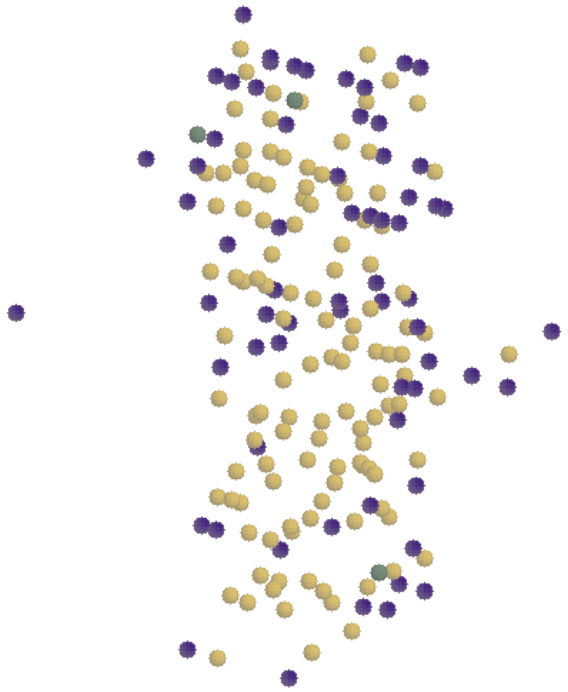

Fig. 3. Distorted cations after the DC (cations with angular distortion in their first neighboring shell); Si (yellow), Zr (blue), U (green).

calculated its number of oxygen neighbors and classified as 'disordered' the cations for which the result differs from what it is in the perfect crystal (see Fig. 2). Such cations are situated in a surrounding very different from what it was in the perfect crystal. Cations with the same number of neighbors as in the crystal are subsequently classified as 'distorted' if the angular distribution around them, measured as the mean square deviation from the perfect crystal, is larger than the value in the perfect crystal under thermal equilibrium at room temperature (see Fig. 3) [27]. The environment of these cations is different from the perfect crystalline one, but much less than for disordered atoms. For each cascade the numbers of disordered and distorted cations are given in Table 5. Both silicon and zirconium ions can experience a disordered surrounding. Nearly all disordered silicon atoms have five oxygen neighbors. The zirconium and uranium ions are much more often disordered than the silicon ions. They exhibit a decrease in their coordination number. Looking at the positions of the disordered and distorted cations in space (Figs. 2 and 3) one can see that disordered Si are located in the very center of the track, while disordered Zr and distorted Si are more spread. Distorted Zr only appear in the outer part of the track. Thus the final configurations of the DC track appears as the superposition of concentric areas, the local amorphous character of which decreases when one goes from its center to the outer undisturbed crystal.

Comparing the quenched configuration potential energies at the beginning and at the end of the simulation, we can calculate the energy stored during the DC (see Table 5). They range between 200 and 479 eV. One can see that most of the introduced energy (4 or 5 keV) has been thermally dissipated and that less than 10% has been stored by the material.

The general (concentrical) shape of the DC tracks is independent of uranium doping. The same kind of local atomic arrangement is also observed for any doping. Nevertheless some differences appear for the global quantities calculated after the cascade. One can see in Table 5 that the swelling is larger in the undoped boxes. In the same way the stored energy seems to decrease with doping. Another difference is the longer cooling time observed in doped boxes.

5. Discussion

5.1. Nature of the amorphous tracks

The amorphous structure and characteristics of the DC tracks were compared to the structure of a globally amorphous zircon. To obtain a model of amorphous zircon, a box containing 5184 atoms initially in a crystalline arrangement was heated up to 14000 K during 25 ps then quenched down to 0 K with a cooling rate of 5×10^{14} K s^{-1}. Due to computer limitations, the present quenching rate is larger by many orders of magnitude with regard to experimental ones. This should be kept in mind since the characteristics of the resulting amorphous zircon may depend on the applied cooling rate. Even if the quenching rate is very high, a box heated up to 5000 K only, recovers a crystalline structure when it is quenched. The cation distortion and disorder tests were applied on the final configuration (see Table 6).

Comparing the characteristics of our model of completely amorphized structure and the ones of the DC tracks, we did not find noticeable differences between the cores of our calculated DC tracks and our model of amorphous material. As in the DC tracks, silicon atoms are either disordered or distorted and zirconium atoms are disordered. Nearly all disordered silicon atoms have five oxygen neighbors. The occurrence of such a surrounding for silicon ions is quite uncommon for silicas but may be observed in some minerals. Their presence in the quenched material is probably due to the too fast cooling. In the DC tracks, it is not clear whether their occurrence is realistic or results from a weakness in our empirical potentials. If such species do exist in real tracks they should probably disappear some time after the DC, but within a time scale that cannot be reached by MD simulations. Disordered zirconium ions in the tracks experience a decrease in their coordination number. This is coherent with the calculated structure of globally amorphous zircon, where all zirconium atoms have less neighbors than in the crystalline one, the mean number of oxygen neighbors decreasing to 6.5. This is in good agreement with extended X-ray absorption fine structure (EXAFS) experiments on amorphous zircon [28] where an approximate value of 7.0 for the number of neighbors has been found. It can also be related to what is observed for the most stable phase of ZrO_2 [29] where the Zr ions are surrounded by seven ions. In the same way, EXAFS experiments show that Zr in nuclear glasses is surrounded by around 6.3 neighbors [30].

The physical origin of this higher number of disordered zirconium atoms compared to silicon atoms comes from the difference in cation–oxygen bonding. Si–O bonding is partially covalent and so the tetrahedral unit is highly energetically favored. In contrast the Zr–O bonding is more ionic and the Zr ions should be seen as trapped in oxygen cages, so a variation in their number of neighbors is less demanding from the energetic point of view. In the framework of BMH potentials the physical difference is mimicked by the different depth and distance of the well in the oxygen cation pair potential. The main difference between bulk amorphous zircon and the cascade tracks is the fact that very few distorted zirconium atoms exist in bulk amorphous zircon. Thus their occurrence is characteristic of the structure of the DC tracks. Distorted zirconium atoms are mainly found on the borders of the tracks. They

Table 6
Characteristics of fully amorphous zircons[a]

Si atoms			Zr atoms		
Crystalline	Distorted	Disordered	Crystalline	Distorted	Disordered
26%	39%	34%	6%	0.5%	93%

[a] Crystalline denotes atoms which are neither distorted nor disordered.

evidence the presence of an accommodation zone between the core of the DC, which has a really amorphous structure, and the outer crystalline structure. Thus the interface between amorphous and crystalline material is not abrupt. DC tracks appear as the superposition of concentric areas of decreasing amorphous character. In their very core both Si and Zr cations are disordered. This area is very much like fully amorphous zircon. In an intermediate shell only distortion is visible on Si ions and Zr ions are disordered. Finally, in the outer shell, only Zr ions are distorted.

5.2. Stored energy

The calculated energy difference between the bulk amorphous and crystalline structures is 0.09 eV per atom. This value is in very good agreement with the experimental figure of 0.10 eV per atom estimated by Ellworth et al. [31]. They measured the energy needed to anneal metamict zircon to its crystalline state at room temperature using transposed temperature drop calorimetric measurements. They obtained a value of −59 kJ mol^{-1} which corresponds to a stored energy of 0.10 eV per atom in the amorphous state.

To compare the energy stored during a DC with the excess energy of the bulk amorphous material one should define the number of ions in the amorphous state after the DC to get a stored energy per atom. Looking at the final structure of the material and at the positions of disordered and distorted atoms it appears that the best way to characterize or delimit the amorphous zone is to define it as the zone filled with disordered zirconium atoms. The number of atoms in the amorphous state is thus defined as six times the number of disordered zirconium ions. With this estimation of the number of atoms in the amorphous state, we can estimate the stored energy per atom after the DC and compare directly this figure with the value calculated in the bulk amorphous material. The obtained figures are of the correct order of magnitude but notably too high (see Table 5). However the stored energy per atoms tends to decrease as the DC energy increases. Two explanations can be put forward to explain this decrease and the overestimation of the stored energies. First it can be an interface effect, the relative importance of the energy stored at the interface being all the more important as the amorphous volume is small. It can also be the evidence for a better annealing of the defects in the high energy cascades due to a higher internal temperature for instance. It is not possible with the present calculations to decide which effect is predominant.

5.3. Decomposition in SiO_2 and ZrO_2

Partial or complete decomposition of zircon in SiO_2 and ZrO_2 is frequently observed as an intermediate stage in annealing experiments of metamict zircons [8]. Direct decomposition under irradiation performed at high temperature has also been observed in an ion bombardment experiment [9]. We tried to estimate whether the beginnings of a such a decomposition in SiO_2 and ZrO_2 can be seen in our calculation. In the perfect crystalline zircon structure, the SiO_4 tetrahedra are disconnected from each other. All oxygen ions are connected to only one silicon atom. Thus the appearance of a SiO_2 phase can be characterized by the existence of oxygen bridging two silicon atoms. So we calculated, on the configuration quenched at the end of the DC, the number of oxygen ions having zero or two silicon neighbors. Fig. 4 represents oxygen and silicon atoms involved in a Si–O–Si bridging. From these calculations, we can define a connectivity index (or polymerization index) for the silicon atoms. For each silicon atom we define this index as the number of its oxygen neighbors connected to another silicon atoms. In the perfect zircon structure this index is equal to zero for all silicon atoms and in quartz it is equal to 4. This index is the same as the one defined in nuclear magnetic resonance or Raman spectroscopy experiments on silica glasses where it is noted Q_4, Q_3, ... for silicon connected to 4, 3, ... other silicon atoms. In the quenched configuration at the end of the cascades we find connectivity indexes varying from Q_0 to Q_5 (see Table 7). The very rare Q_5 silicon atoms are clearly a non physical aberration of the empirical potentials probably due to the absence of three bodies terms. Q_0 corresponds to the unconnected tetrahedra of the zircon crystalline structure. Silicon atoms with a polymerization index larger than Q_3 evidence the appearance of a SiO_2 nanophase. Q_1 or Q_2 silicon atoms can either be situated at the border of SiO_2 nanophases or isolated groups. The number of highly polymerized silicon depends strongly on the initial kinetic energy of the projectile. The intra-tetrahedral configurations around the silicon atoms are widely distorted compared

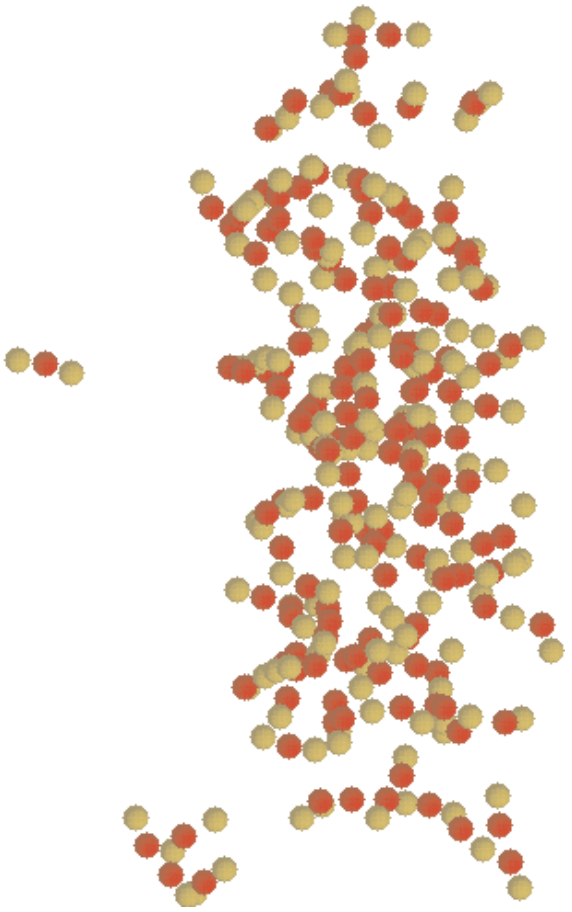

Fig. 4. View of the SiO_2 nanophase built from Si–O–Si bonding; Si (yellow), O (red).

to silica tetrahedra. The inter-tetrahedral arrangement is also very distorted. Indeed a few edge-sharing (and even face-sharing) tetrahedra appear when only corner-sharing tetrahedra exist in silicas. This, as well as the occurrence of Q_5 silicon atoms, proves that the SiO_2 nanophase that comes out of our calculations is still very far from its equilibrium configuration at the end of the simulation. The equilibration of the atomic positions would continue to proceed after the first few ten picoseconds but it certainly takes place on a time scale much too large for MD simulations.

Besides, comparing bulk amorphous material and DC tracks, one can see that the same linkage between SiO_n polyhedra that appears in the DC tracks exists in the amorphous material (Table 7) High polymerization indexes are more common in the globally amorphized structure than in the DC tracks. This is probably due only to the small size of the DC tracks cores, the silicon atoms situated at the interface between amorphous and crystalline regions having necessarily a smaller connectivity index. Thus the cores of the tracks exhibit the same kind of nanophases that exist in bulk amorphous zircons.

Our calculations clearly evidence the appearance of SiO_2 and ZrO_2 nanophases immediately after the DC. The evolution of these SiO_2 and ZrO_2 nanophases would determine whether an effective decomposition is eventually triggered or not under irradiation; but MD calculations cannot give insight into such a long time evolution. Meldrum et al. [9] suggest that decomposition under irradiation is driven by thermally activated diffusion inside the thermal spike formed by the DC. We cannot conclude about this point. We indeed find that the temperature reached inside the track during the cascade is much higher than the decomposition temperature for about 1 ps and remains higher than the decomposition temperature for a few picoseconds which a very short time for thermally activated diffusion events. Yet one should keep in mind that the cooling rate in our calculations depends strongly on the size of the box. It also remains unclear whether the decomposition under irradiation is only due to the local high temperature or whether the irradiation itself plays a role, beyond the thermalization of the track. For instance irradiation accelerated diffusion may be important for this decomposition.

Table 7
Number of silicon atoms with a given connectivity index Q_i, measured in the DC tracks [a]

Cascade number	Polymerization index					
	Q_0	Q_1	Q_2	Q_3	Q_4	Q_5
1		35	26	15	3	
2		64	51	33	14	3
3		39	34	12	2	1
4		71	57	27	9	
5		85	55	31	11	4
Amorphous zircon	4%	17%	29%	29%	16%	5%

[a] The cascade number is the same as in Table 5. For comparison we note in the last line the percentages of the different connectivities found for bulk amorphous zircon.

5.4. Global amorphization process

The most important effect of irradiation in zircon is the global transition from crystalline to amorphous state. The global amorphization process is quite complicated as it involves many cascades and the creation of defects (either point defects or larger defects), and their recoiling either through thermal activation or mediated by subsequent irradiation. Many phenomenological models exist for such a phenomenon [32], see [33] for an application of these models for zircon. They tend to classify the amorphization processes as (the following list is not exhaustive):

- direct impact processes where the amorphization is achieved directly within a cascade.
- single (double, multiple) overlap processes where the overlap of two (three, many) cascades, each cascade producing a certain amount of point defects, are needed to amorphize an area of the crystal.
- composite models where a cascade produces a central amorphous zone and peripheral damaged zones subject to further amorphization by overlapping of subsequent cascades.

From an analysis of the variation of the macroscopic swelling of zircon with irradiation dose, Weber et al. [10] claimed that amorphization follows the double overlap model. Nevertheless, recent X-ray diffraction experiments [34] tend to show that amorphization occurs through direct impact inside the DC tracks. Our calculations are more in favor of the direct impact model as they exhibit an amorphous core in the DC tracks and no point defect. However, it remains possible that the peripheral zones of the tracks with smaller disorder become fully amorphized when overlap occurs. Anyway it is clear from our calculations that the correct model for amorphization should include the presence of amorphous cores produced by single cascades.

6. Conclusions

We have used MD with BMH pair potentials to study irradiation damage in zircons. DTE have been calculated and DC initiated by α-decay recoil nuclei have been modeled. Threshold displacement energies are different for each ion type and much higher for cations than for oxygen ions. The calculated DC clearly exhibit amorphous tracks of concentrical shape. In the center of the track, cation surroundings are highly disordered. This area has the structure of fully amorphous zircon. A mooth interface area exists between the fully amorphous core of the DC tracks and the perfectly crystalline surrounding medium. The track exhibits less and less disorder from the core to the outer shell of the track. In the amorphous zone, some silicon tetrahedra are connected to each other indicating the appearance of SiO_2-rich and ZrO_2-rich nanophases. These nanophases should play a role in the observed decomposition of zircon in annealing and ion bombardment experiments.

Acknowledgements

Dr Jean-Marc Delaye and Dr Laurent Veiller are thankfully acknowledged for many fruitful discussions and reading of the manuscript.

References

[1] R.C. Ewing, W. Lutze, W.J. Weber, J. Mater. Res. 10 (1995) 243.
[2] M.T. Robinson, J. Nucl. Mater. 216 (1994) 1.
[3] R.C. Ewing et al., Prog. Nucl. Energy 29 (1995) 63.
[4] H.D. Holland, D. Gottfried, Acta Crystallogr. 8 (1955) 291.
[5] B.C. Chakoumakos, et al., Radiat. Eff. Def. Solids 118 (1991) 393.
[6] R.C. Ewing et al., in: W. Lütze (Ed.), Scientific Basis for Radioactive Waste Management V, North-Holland, New York, 1982.
[7] E.M. Levin, H.F. McMurdie, Phase diagrams for Ceramist 1975 Supplement, American Ceramic Society, Colombus, OH, 1975.
[8] H. Zhang et al., J. Phys. 12 (2000) 3131.
[9] A. Meldrum, S.J. Zinkle, L.A. Boatner, R.C. Ewing, Nature 395 (1998) 56.
[10] W.J. Weber, R.C. Ewing, L. Wang, J. Mater. Res. 9 (1994) 688.
[11] J.F. Ziegler, J.P. Biersack, U. Littmark, Stopping Powers and Ranges in All Elements, vol. 3, Pergamon, NewYork, 1977.
[12] B.G. Dick, A.W. Overhauser, Phys. Rev. 112 (1958) 90.
[13] S.W. De Leeuw et al., Proc. R. Soc. Lond. A 373 (1980) 27.
[14] L. Verlet, Phys. Rev. 159 (1967) 98.
[15] N.V. Doan, H. Tietze, Nucl. Instrum. and Meth. B 102 (1995) 58.
[16] J.M. Delaye, D. Ghaleb, J. Non-Cryst. Solids 195 (1996) 239.
[17] J.M. Delaye, D. Ghaleb, J. Nucl. Mater. 244 (1997) 22.
[18] J.-M. Delaye, D. Ghaleb, Phys. Rev. B 61 (2000) 14481.
[19] J.-P. Crocombette, D. Ghaleb, J. Nucl. Mater. 257 (1998) 282.
[20] J.-P. Crocombette, Phys. Chem. Miner. 27 (1999) 138.
[21] K. Robinson et al., Am. Mineral. 56 (1971) 782.
[22] S.J. Zinkle, C. Kinoshita, J. Nucl. Mater. 251 (1997) 200.
[23] R. Devanathan et al., Mater. Res. Soc. Symp. Proc. vol. 481, p. 419.
[24] R. Williford et al., Nucl. Instrum. and Meth. B 141 (1998) 94.
[25] C. Meis (CE Saclay France), private communication.
[26] M. Parinello, A. Rahman, J. Appl. Phys. 52 (1981) 7182.
[27] H. Zhu, R.S. Averback, M. Nastasi, Philos. Mag. A 71 (1995) 735.

[28] F. Farges, Phys. Chem. Miner. 20 (1994) 504.
[29] R. Wyckoff, Crystal Structures, Interscience, New York, 1951.
[30] L. Galoisy et al., J. Am. Ceram. Soc. 82 (8) (1999) 2219.
[31] S. Ellsworth et al., Phys. Chem. Miner. 21 (1994) 140.
[32] R. Webb, G. Carter, Radiat. Eff. 42 (1979) 159.
[33] W.J. Weber, J. Mater. Res. 5 (1995) 2687.
[34] S. Rio et al., J. Phys. 12 (2000) 2401.